IEEE Access
Multidisciplinary | Rapid Review | Open Access Journal

Received January 26, 2019, accepted February 12, 2019, date of publication February 25, 2019, date of current version March 8, 2019.

Digital Object Identifier 10.1109/ACCESS.2019.2900284

Frequency Estimator Based on Spectrum Correction and Remainder Sifting for Undersampled Real-Valued Waveforms

XIANGDONG HUANG[1], (Member, IEEE), HUIJIE WANG[1], HAOHUA QIN[1], AND WEIZHI NIE[2], (Member, IEEE)

[1]School of Electrical and Information Engineering, Tianjin University, Tianjin 300072, China
[2]College of Automation and Electronic Engineering, Qingdao University of Science and Technology, Qingdao 266000, China

Corresponding author: Weizhi Nie (weizhinie@163.com)

This work was supported by the National Natural Science Foundation of China under Grant 61671012.

ABSTRACT Frequency estimation of undersampled waveforms receives increasing attention in communication, radar signal processing, instrumentation and measurements, and so on. However, due to the lack of recognizing the correct remainder between two side spectra, the existing Chinese Remainder Theorem (CRT)-based frequency estimators can hardly deal with real-valued signals. To achieve this goal, this paper proposes an estimator combining spectrum correction (aiming to enhance reconstruction accuracy by incorporating the fractional parts of DFT remainders), closed-form CRT, and a remainder sifting approach. Based on the detection of an undersampled waveform's zero crossing point, this solution can pick out the correct remainder between two side spectra, which ensures that the CRT achieves a valid reconstruction. Compared with the existing Maroosi-Bizaki estimator, the proposed method not only enlarges the upper bound of frequency recovery but also possesses higher reconstruction accuracy (the relative error is less than 0.002%) with lower consumption of computational complexity. The numerical results verify the superior performances of our estimator.

INDEX TERMS Frequency estimation, real-valued undersampled waveforms, remainder sifting, spectrum correction.

I. INTRODUCTION

Frequency estimation of a high-frequency sinusoidal waveform is widely encountered in mobile communication, instrumentation and measurements, spectrum sensing in cognitive radio etc. However, when the signal frequency reaches a high degree, limited by the contradiction between the Nyquist sampling rate and the hardware-realizable ADC (Analog to Digital Converter), both the power consumption and the hardware cost get increasingly large. In some particular circumstances (such as the sampling rate $f_s > 10^9$ samples/s), it is even unrealizable. For example, the received signals in the velocity synthetic aperture radar [1] may be of undersampled nature. Accordingly, frequency estimation has to be implemented in undersampled condition rather than in Nyquist sampling condition. In addition, the problem of phase unwrapping, involved in radar signal processing and sensor networks [2], [3], is essentially a particular case of undersampled measurement, also. To emphasize, in these measurements, undersampling from real waveforms is preferred to complex ones due to hardware source limitation. Hence, it is urgent to develop an approach to achieve frequency estimation from undersampled real-valued samples.

Maroosi and Bizaki proposed a searching-matching based frequency estimator [4], [5] for undersampled real-valued waveforms, in which the frequency estimate is determined by applying the *the minimax-distance* criterion (see [4]) to find out an optimal remainder combination among a pre-set searching space. Nevertheless, this space consists of all the direct remainders and their derived eligible remainders (i.e., plus integers times of the corresponding undersampling rate) and thus it is very large, which renders heavy searching complexity to this estimator. Moreover, as [4] pointed out, the upper bound of realizable frequency estimator of this

The associate editor coordinating the review of this manuscript and approving it for publication was Bora Onat.

2169-3536 © 2019 IEEE. Translations and content mining are permitted for academic research only.
Personal use is also permitted, but republication/redistribution requires IEEE permission.
See http://www.ieee.org/publications_standards/publications/rights/index.html for more information.

estimator is a bit low. Besides, Huang and Zhang [6] derived a three sub-Nyquist channels based estimator. However, the upper bound of realizable frequency is not sufficiently high and its fundamental is on basis of the complex signal model rather than the real-valued model.

Chinese Remainder Theorem (CRT) is another efficient approach to estimate frequencies of undersampled waveforms. Specifically, given L moduli $M_1, \ldots, M_L$, CRT can recover an integer number f from L remainders $r_1, \ldots, r_L$,

$$r_i \equiv f \mod M_i, \quad i = 1, \ldots, L, \tag{1}$$

where 'f' stands for the high frequency to be measured, $M_1, \ldots, M_L$ refer to the moduli (correspond to sub-Nyquist sampling rates [7]) and $r_1, .., r_L$ represent the remainders of L moduli $M_1, \ldots, M_L$ (thus $0 \leq r_i < M_i$). Hence, the conventional CRT has been applied in co-prime spectrum sensing (see [8], [9] for details) to explore the spectral characteristic of undersampled waveforms. However, this estimator suffers from large latency [8], [10] and high complexity.

In recent years, a lot of improved algorithms [11]–[13], have been developed to reduce CRT's complexity and improve CRT's robustness. Up to now, the state-of-the-art CRT algorithms (the closed-form CRT in [14]–[17]) can bypass the conventional CRT's searching operation and they also possess a higher reconstruction accuracy, which greatly enhances CRT-based estimators' practicability.

However, there are two improvable points for these improved CRT estimators.

On one hand, these estimators can only handle undersampled complex exponential signals, and they will fall into failure when dealing with real-valued sinusoidal waveforms. This arises from the fact that, for each channel, CRT only requires a single DFT remainder. Nevertheless, a real-valued signal has two side spectra which provide two candidates of DFT remainder. Accordingly, L channels of real-valued waveforms generate $2L$ remainders. Hence, the core problem is to sift L remainders from these $2L$ remainders.

On the other hand, these estimators only consider those frequencies whose fractional parts of DFT remainders equal zero (like [11] does) or ignore the fractional parts of DFT remainders (for example, the fractional part ε_i of a DFT remainder is discarded in [18]), which inevitably degrades the accuracy of frequency estimation.

To solve these two problems, this paper proposes an improved CRT-based estimator, which can sift the desired remainders from the DFT spectra of real-valued signals through combining spectrum correction with phase matching, rendering our estimator with the ability of dealing with real-valued sinusoidal waveforms. Due to the consideration of detecting an undersampled waveform's zero crossing point (not required by the determination algorithm addressed in [4]), the recoverable frequency can reach the same upper bound as the determination case of complex exponential waveforms.

With the above techniques incorporated, the proposed estimator not only acquires a larger reconstruction range than the estimators proposed in [4], [5], and [6], but also improves the reconstruction accuracy and widens the application range of the existing CRT-based estimators.

The remainder of this work is structured as follows: firstly, we build up a CRT-based estimator model for the frequency estimation of undersampled real-valued waveforms. Secondly, details on how to sift the desired DFT remainders by means of spectrum correction and remainder sifting are addressed. Thirdly, numerical results are presented and finally conclusions are drawn.

II. CRT-BASED ESTIMATION MODEL OF REAL-VALUED WAVEFORMS

A. SIGNAL MODEL

Consider a high-frequency sinusoidal signal $x(t)$ formulated as

$$x(t) = a\cos(2\pi ft + \theta_0), \tag{2}$$

where a, θ_0 and f are the amplitude, initial phase and the frequency to be determined, respectively. Suppose that L undersampling rates $f_{s1}, \ldots, f_{sL}$ are specified as

$$f_{si} = N\Gamma_i, \quad i = 1, \cdots, L, \tag{3}$$

where the gcd (great common divisor) of any pair Γ_i and Γ_j for $i \neq j$ is 1 [19] and thus N exactly equals the gcd of the integer group $\Gamma_1, \cdots, \Gamma_L$. Note that, the channel number L is an integer not smaller than 1 (i.e., $L \in \{2, 3, 4, \ldots.\}$).

Accordingly, the i-th undersampled sequence $x_i(m)$, $i = 1, \cdots, L$, is

$$x_i(m) = a\cos(2\pi f_0/f_{si}m + \theta_0), \quad m = 0, \cdots, N-1. \tag{4}$$

Hence, the individual frequency f_i of $x_i(m)$ can be written as

$$f_i = \frac{f_0}{f_{si}} = n_i + \frac{k_i}{N} + \frac{\delta_i}{N}, \quad 1 \leq i \leq L \tag{5}$$

where n_i is the unknown folding integer, k_i refers to the index of the peak DFT bin and δ_i is a fractional frequency offset, i.e.,

$$k_i \in \{0, 1, \ldots, N-1\}, \quad |\delta_i| \leq 0.5. \tag{6}$$

Therefore, (5) can be converted into a simultaneous congruence equation as

$$\begin{cases} f_0 = n_1 f_{s1} + (k_1 + \delta_1) f_{s1}/N \\ f_0 = n_2 f_{s2} + (k_2 + \delta_2) f_{s2}/N \\ \qquad\qquad \vdots \\ f_0 = n_L f_{sL} + (k_L + \delta_L) f_{sL}/N. \end{cases} \tag{7}$$

Eq. (7) shows that, frequency estimation in (5) is equivalent to CRT reconstruction, in which $f_{s1}, \ldots, f_{sL}$ refer to moduli and the second terms on the right hand side of (7) refer to remainders $r_1, \ldots, r_L$, i.e.,

$$r_i = \frac{(k_i + \delta_i)}{N} \cdot f_{si}, \quad 1 \leq i \leq L. \tag{8}$$

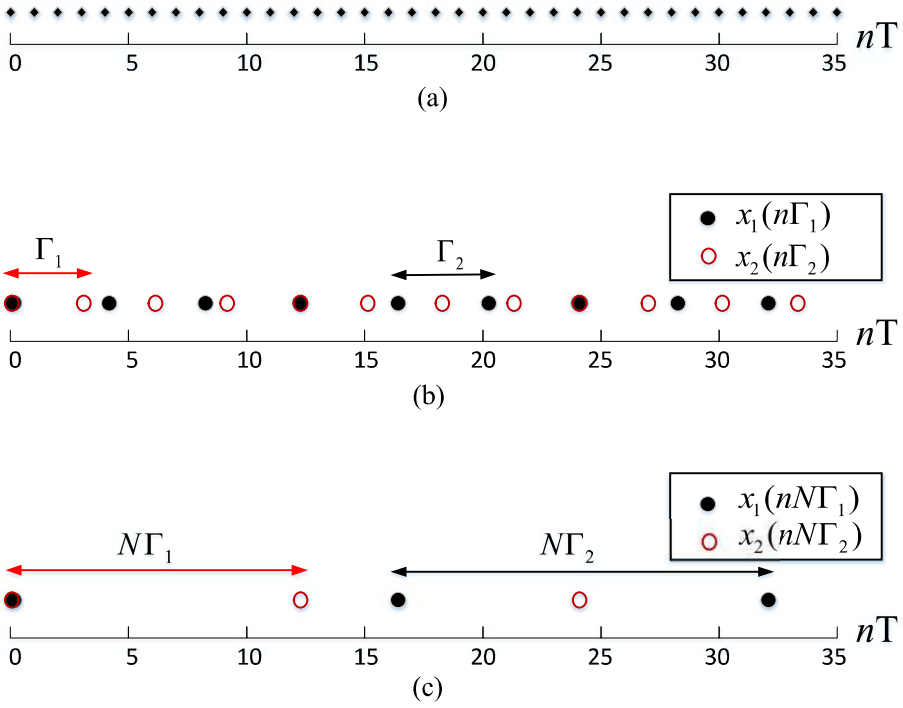

FIGURE 1. 3 kinds of sampling structures ($\Gamma_1 = 3, \Gamma_2 = 4, L = 2$). (a) Case of Nyquist sampling. (b) Case of conventional coprime undersampling. (c) Case of proposed coprime undersampling ($N = 4$).

In fact, the fractional part δ_i in r_i was ignored by the existing estimators in [7], [11], [12], and [3], [18], [19], thereby inevitably degrading the reconstruction accuracy. Also, these estimators only address the frequency estimation of undersampled complex exponential signals and do not take real-valued sinusoidal signals into account.

B. SAMPLING STRUCTURE AND RECONSTRUCTION RANGE

In terms of (2)-(4), the sampling structure of the proposed estimator is illustrated in Fig. 1(c). Besides, the sampling structures for the case of Nyquist sampling and the conventional coprime sampling are also plotted in Fig. 1(a), (b), respectively.

As Fig. 1 (b) depicts, the sampling intervals at two undersampling channels are Γ_1, Γ_2, whereas the sampling intervals of the sampling structure in Fig. 1 (c) are $N\Gamma_1, N\Gamma_2$. Therefore, this sampling structure exhibits a much more sparse distribution.

On the contrary, for estimators with distinct sampling structures, if their ADC sampling rates are at the same amount level, the proposed estimator surely acquires a higher reconstruction range. As [19] proved out, the upper bound $f_{\max}$ of CRT reconstruction with the sampling structure in Fig. 1 (c) is the least common multiple of all moduli, i.e.,

$$f_{\max} = N \prod_{i=1}^{L} \Gamma_i. \tag{9}$$

Specifically, for the case $L = 3$, our proposed estimator's upper bound $f_{\max} = N\Gamma_1\Gamma_2\Gamma_3$, compared to that $f_{\max}$ only equals $\Gamma_1\Gamma_2\Gamma_3$ for the estimator in [6].

III. THE PROPOSED ESTIMATOR

A. PRINCIPLE OF IDEAL PHASE RECOVERY USING SPECTRUM CORRECTION

Combining (4) with (5), one can further rewrite the undersampled sequence $x_i(m)$ as

$$\begin{aligned} x_i(m) &= a\cos[2\pi(n_i + (k_i + \delta_i)/N)m + \theta_0] \\ &= \frac{a}{2}[e^{j\omega_i m}e^{j\theta_0} + e^{-j\omega_i m}e^{-j\theta_0}] \\ &= \frac{a}{2}[e^{j\omega_i m}e^{j\theta_0} + e^{j(2\pi-\omega_i)m}e^{-j\theta_0}], \\ \omega_i &= (k_i + \delta_i)2\pi/N, \quad 1 \le i \le L. \end{aligned} \tag{10}$$

Eq (10) shows that, for a real-valued sinusoidal signal $x(t)$, each undersampled version $x_i(m)$ contains two conjugate components. Their frequencies are complement (ω_i and $2\pi - \omega_i$) and their phases are opposite (θ_0 and $-\theta_0$). In particular, only the component ω_i rather than its complement component $2\pi - \omega_i$ provides the true DFT remainder. As a result, for a single channel, there exists an ambiguity in distinguishing the true remainder component ω_i from the fake component $2\pi - \omega_i$.

Further, this ambiguity gets more complex among multiple undersampling channels. Particularly, for the i-th channel, if $k_i < N/2$, then, ω_i is located at the left half-spectrum and $2\pi - \omega_i$ falls at the right half-spectrum. On the contrary, if $N/2 + 1 \le k_i \le N - 1$, then ω_i is located at the right

half-spectrum and $2\pi - \omega_i$ falls at the left half-spectrum. Hence, for two different channels i_1, i_2 ($i_1 \neq i_2$), it is very likely that their DFT remainder components ω_{i_1} and ω_{i_2} fall at two distinct half-spectra, respectively. Only when all the true components $\omega_1, \cdots, \omega_L$ are correctly recognized (i.e., the fake components $2\pi - \omega_1, \cdots, 2\pi - \omega_L$ are discarded) can the subsequent CRT achieve frequency estimation for real-valued waveforms.

It can be inferred from (10) that, for any channel, whether the true remainder component ω_i is located within the left half-spectrum or the right half-spectrum, its phase value theoretically equal θ_0. In other words, practically, this expected component ω_i can be recognized by identifying whether its detection phase approximates the ideal value θ_0 or not.

However, due to a nonzero frequency offset δ_i, the DFT detection phase always deviates from the ideal value θ_0. To explain this, we can deduce the DTFT result $X_i(j\omega)$ of $x_i(m)$ in (10) as

$$X_i(j\omega) = \frac{a}{2}\left\{\frac{\sin\left[(\omega-\omega_i)N/2\right]}{\sin\left[(\omega-\omega_i)/2\right]}e^{j\left[\theta_0-\frac{N-1}{2}(\omega-\omega_i)\right]} + \frac{\sin\left[(\omega+\omega_i)N/2\right]}{\sin\left[(\omega+\omega_i)/2\right]}e^{j\left[-\theta_0-\frac{N-1}{2}(\omega+\omega_i)\right]}\right\}. \quad (11)$$

Since the DFT result $X_i(k)$ is no more than the equi-spaced sampled version of DTFT, i.e.,

$$X_i(k) = X_i(j\omega)\big|_{\omega=k2\pi/N}, \quad k = 0, \cdots, N-1. \quad (12)$$

Therefore, substituting (11) and $\omega_i = (k_i + \delta_i)2\pi/N$ into (12) yields

$$X_i(k) = \frac{a}{2}\left\{\frac{\sin\left[\pi(k-k_i-\delta_i)\right]}{\sin\left[\pi(k-k_i-\delta_i)/N\right]}e^{j\left[\theta_0-\frac{\pi(N-1)}{N}(k-k_i-\delta_i)\right]} + \frac{\sin\left[\pi(k+k_i+\delta_i)\right]}{\sin\left[\pi(k+k_i+\delta_i)/N\right]}e^{j\left[-\theta_0-\frac{\pi(N-1)}{N}(k+k_i+\delta_i)\right]}\right\}. \quad (13)$$

Recall that the peak DFT bins of two half-spectra are respectively at $k = k_i$ and $k = N - k_i$. Either $X_i(k_i)$ or $X_i(N - k_i)$ consists of two terms sampled from the well-known function $\sin(\pi x)/\sin(\pi x/N)$. What's more, one term is sampled within the mainlobe interval $(-1, 1)$, whereas the other term is sampled outside this interval. Since $\sin(\pi x)/\sin(\pi x/N)$ tends to be 0 when x gets farther away from the mainlobe interval $(-1, 1)$, the interference between these two half-spectra can be ignored. Thus, one can approximately deduce $X_i(k_i)$ and $X_i(N - k_i)$ as

$$X_i(k_i) \approx \frac{a}{2}\cdot\frac{\sin(\delta_i\pi)}{\sin(\delta_i\pi/N)}e^{j[\theta_0+\delta_i(N-1)\pi/N]},$$
$$X_i(N-k_i) \approx \frac{a}{2}\cdot\frac{\sin(\delta_i\pi)}{\sin(\delta_i\pi/N)}e^{j[-\theta_0-\delta_i(N-1)\pi/N]}. \quad (14)$$

Hence, the observation phases of $X_i(k_i)$ and $X_i(N - k_i)$ are approximately denoted as

$$\phi(k_i) \approx \theta_0 + \delta_i(N-1)\pi/N,$$
$$\phi(N-k_i) \approx -\theta_0 - \delta_i(N-1)\pi/N. \quad (15)$$

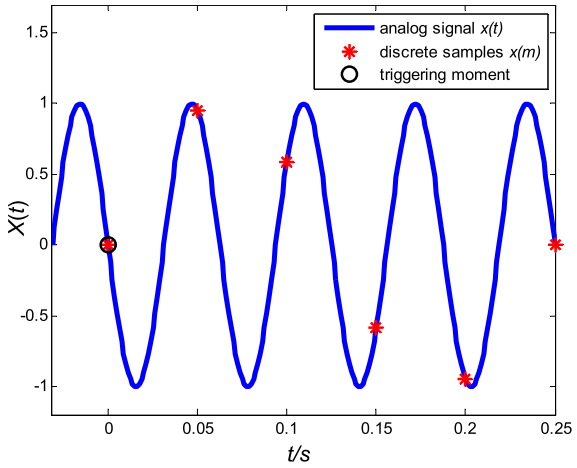

FIGURE 2. Samples triggered with the initial phase $\pi/2$ at an individual channel.

Eq (15) shows that, the ideal phase θ_0 (or its opposite version) can be recovered from two peak DFT bins' observation phases $\phi(k_i)$ and $\phi(N - k_i)$, i.e.,

$$\hat{\theta}_0 \approx \phi(k_i) - \delta_i(N-1)\pi/N,$$
$$-\hat{\theta}_0 \approx \phi(N-k_i) + \delta_i(N-1)\pi/N. \quad (16)$$

From (16), one can find that, for the purpose of recovering the ideal phase, the unknown frequency offset δ_i needs to be estimated. This can be realized by some frequency correctors (such as Quinn corrector [20], Candan corrector [21], phase-difference corrector [22] etc.). For example, if the remainder component is determined at $k = k_i$, then the Candan corrector provides the estimate of δ_i as

$$\hat{\delta}_i = \frac{\tan(\pi/N)}{\pi/N}\cdot\text{Real}\left\{\frac{X_i(k_i-1) - X(k_i+1)}{2X_i(k_i) - X_i(k_i-1) - X_i(k_i+1)}\right\}. \quad (17)$$

The problem lies in identifying whether $k = k_i$ falls in the left half-spectrum or in the right half-spectrum. The following method of remainder sifting can achieve this task.

B. REMAINDER SIFTING APPROACH

In fact, the initial phase θ_0 in (2) is practically easy to be determined by circuit detection. As Fig. 2 depicts, if we employ a triggering circuit to detect the zero crossing point 'O' (exactly passing from positive to negative) of the original analog waveform $x(t)$ and then simultaneously start the subsequent undersampling operations of all L channels. Therefore, for any channel, its undersampled sequence acquires an initial phase $\theta_0 = \pi/2$. Then, remainder sifting can be realized by the following procedure of phase matching.

Firstly, for the i-th channel, use a spectrum corrector on the left-half-spectrum peak DFT bin $X_i(k_{i,L})$ to generate the estimate $\hat{\delta}_i$ of the frequency offset. In terms of (16), two corrected phases $\hat{\varphi}_{i,L}, \hat{\varphi}_{i,R}$ can be calculated as

$$\hat{\varphi}_{i,L} = \phi_{i,k_{i,L}} - (N-1)/N\cdot\hat{\delta}_i\cdot\pi. \quad (18)$$

$$\hat{\varphi}_{i,R} = \phi_{i,k_{i,R}} + (N-1)/N \cdot \hat{\delta}_i \cdot \pi. \tag{19}$$

Secondly, matching the corrected phases $\hat{\varphi}_{i,L}, \hat{\varphi}_{i,R}$ with the known triggering phase θ_0 to make a decision of k_i between $k_{i,L}$ and $k_{i,R}$ as

$$\hat{k}_i = \begin{cases} k_{i,L}, & if \ \ |\hat{\varphi}_{i,L} - \theta_0| < |\hat{\varphi}_{i,R} - \theta_0| \\ k_{i,R}, & else. \end{cases} \tag{20}$$

Thirdly, the remainder of the i-th channel is estimated as

$$\hat{r}_i = \begin{cases} (\hat{k}_i + \hat{\delta}_i) \cdot f_{si}/N, & if \ \hat{k}_i = k_{i,L} \\ (\hat{k}_i - \hat{\delta}_i) \cdot f_{si}/N, & if \ \hat{k}_i = k_{i,R}. \end{cases} \tag{21}$$

C. SUMMARY OF THE PROPOSED ESTIMATOR

To help readers comprehend the proposed estimator, we integrate the spectrum corrector, the technique of phase matching and the closed-form CRT into a summarized procedure, which consists of the following stages.

Stage 1 Use L ADCs with undersampling rates $f_{s1}, \ldots, f_{sL}$ to discretize the original waveform $x(t)$ at the initial phase triggered by a down zero-crossing point (i.e., $\theta_0 = 90°$).

Stage 2 Implement N-point DFT on all undersampled sequences $\{x_1(m)\} \sim \{x_L(m)\}$ and obtain their DFT spectra $\{X_1(k)\}, \ldots, \{X_L(k)\}$.

Stage 3 Search out the left-half-spectrum peak index $k_{i,L}$ and the right-half-spectrum peak index $k_{i,R}$ of $X_i(k)$. Record their phase observations $\phi_{i,k_{i,L}}$ and $\phi_{i,k_{i,R}}$, $i = 1, \cdots, L$.

Stage 4 Employ a frequency corrector to estimate the frequency offset $\hat{\delta}_i$ and use (18), (19) to calculate two corrected phases $\hat{\varphi}_{i,L}, \hat{\varphi}_{i,R}$. Then, use (20) and (21) to determine the screened peak index $\hat{k}_i$ and the remainder $\hat{r}_i$.

Stage 5 Substitute the moduli $f_{s1}, \ldots, f_{sL}$, the remainders $\hat{r}_1, \ldots, \hat{r}_L$ into the closed-form robust CRT addressed in [19] to obtain the final frequency estimate $\hat{f}$.

The closed-form CRT involved in Step 5 consists of the following steps:

Step 1 Use the remainders $\hat{r}_1, \ldots, \hat{r}_L$ to calculate $L-1$ difference remainders $\hat{q}_{i,1}$ as

$$\hat{q}_{i,1} = \left[\frac{\hat{r}_i - \hat{r}_1}{N} \right], \quad 2 \le i \le L. \tag{22}$$

Step 2 Calculate the remainder of $\hat{q}_{i,1}\bar{\Gamma}_{i,1}$ modulo Γ_i:

$$\hat{\xi}_{i,1} = \hat{q}_{i,1}\bar{\Gamma}_{i,1}\Gamma_{\mathbf{i}}, \quad 2 \le i \le L. \tag{23}$$

where $\bar{\Gamma}_{i,1}$ is the modular multiplicative inverse of Γ_1 modulo Γ_i and can be calculated in advance.

Step 3 Calculate the folding integer $\hat{n}_1$ as

$$\hat{n}_1 = \sum_{i=2}^{L} \hat{\xi}_{i,1} b_{i,1} \frac{\gamma_1}{\Gamma_i} \gamma_{\mathbf{1}}. \tag{24}$$

where $b_{i,1}$ is the modular multiplicative inverse of γ_1/Γ_i modulo Γ_i ($\gamma_1 = \Gamma_2\Gamma_3 \cdots \Gamma_L$).

Step 4 Calculate the other $L-1$ folding integers $\hat{n}_i$:

$$\hat{n}_i = \frac{\hat{n}_1\Gamma_1 - \hat{q}_{i,1}}{\Gamma_i}, \quad 2 \le i \le L. \tag{25}$$

Step 5 Calculate the i-th frequency estimate $\hat{f}_{0,i}$

$$\hat{f}_{0,i} = \hat{n}_i f_{si} + \hat{r}_i, \quad 1 \le i \le L. \tag{26}$$

Step 6 Averaging $\hat{f}_{0,1}, \ldots, \hat{f}_{0,L}$ yields the final estimate $\hat{f}$

$$\hat{f} = \frac{1}{L} \sum_{i=1}^{L} \hat{f}_{0,i}. \tag{27}$$

Now we present an example to explain the above 5 stages of frequency retrieval.

Example 1: Consider an analog signal $x(t) = 2\cos(2\pi f_0 t + \pi/2)$, $f_0 = 748.8$Hz. Suppose that $x(t)$ is parallelly discretized by $L = 3$ ADCs with sub-Nyquist sampling rates $f_{s1} = 128$Hz, $f_{s2} = 192$Hz, $f_{s3} = 320$Hz. Hence, the greatest common divisor $N = \gcd\{f_{s1}, f_{s2}, f_{s3}\} = 64$.

Stage 1: Use 3 ADCs with the undersampling rates 128Hz, 192Hz and 320 Hz to discretize $x(t)$ at the initial phase triggered by a down zero-crossing point (i.e., $\theta_0 = 90°$).

Stage 2: Implement 64-point DFT on 3 undersampled sequences to acquire 3 paths of DFT spectra, whose magnitude spectra $|X_1(k)|, |X_2(k)|, |X_3(k)|$ and phase spectra $\phi_1(k), \phi_2(k), \phi_1(k)$ are plotted in Fig. 3. It can be seen that, severe spectral leakage occurs in each DFT spectrum.

Stage 3: From Fig. 3, one can find that the peak indices $k_{i,L}$, $k_{i,R}$ of $|X_1(k)|, \ldots, |X_3(k)|$ are $\{10, 54\}$, $\{6, 58\}$ and $\{22, 42\}$, respectively. Moreover, as Table 1 lists, their phase observations $\phi_{i,k_{i,L}}$, $\phi_{i,k_{i,R}}$ are $\{-161.30°, 161.30°\}$, $\{-17.27°, 17.27°\}$ and $\{47.08°, -47.08°\}$, which heavily deviate from two ideal phases 90° or −90°.

Stage 4: In terms of the Candan formula (17), one can calculate 3 frequency offset estimates $\hat{\delta}_1 = -0.4010$, $\hat{\delta}_2 = 0.4021$, $\hat{\delta}_3 = -0.2400$, as Table 1 lists. Substituting $\hat{\delta}_1, \hat{\delta}_2, \hat{\delta}_3$ and aforementioned phase observations into (18) yields the following corrected phases $\hat{\varphi}_{i,k}$ values: $\{-90.25°, 90.25°\}$, $\{-88.52°, 88.52°\}$, $\{89.60°, -89.60°\}$. Then, in terms of (20), matching the above corrected phases with the known triggering phase $\theta_0 = 90°$, one can deduce that the true DFT remainder bins are at $\hat{k}_1 = 54$, $\hat{k}_2 = 58$, $\hat{k}_3 = 22$. Further, substituting $\hat{k}_1, \hat{k}_2, \hat{k}_3, \hat{\delta}_1, \hat{\delta}_2, \hat{\delta}_3$ into (21) yields the remainder estimates $\hat{r}_1 = 108.8020$, $\hat{r}_2 = 172.7936$, $\hat{r}_3 = 108.8002$.

Stage 5: Substituting the moduli f_{s1}, f_{s2}, f_{s3}, the remainders $\hat{r}_1, \hat{r}_2, \hat{r}_3$ into the aforementioned 5 steps of the closed-form robust CRT, one can calculate the final frequency estimate $\hat{f} = 748.7986$Hz (compared to the true value $f_0 = 748.80$Hz), as Table 1 lists.

D. DISTINCTIONS BETWEEN THE PROPOSED ESTIMATOR AND THE MAROOSI-BIZAKI ESTIMATOR

As mentioned before, the frequency recovery of undersampled real-valued sinusoidal signals was first solved by the

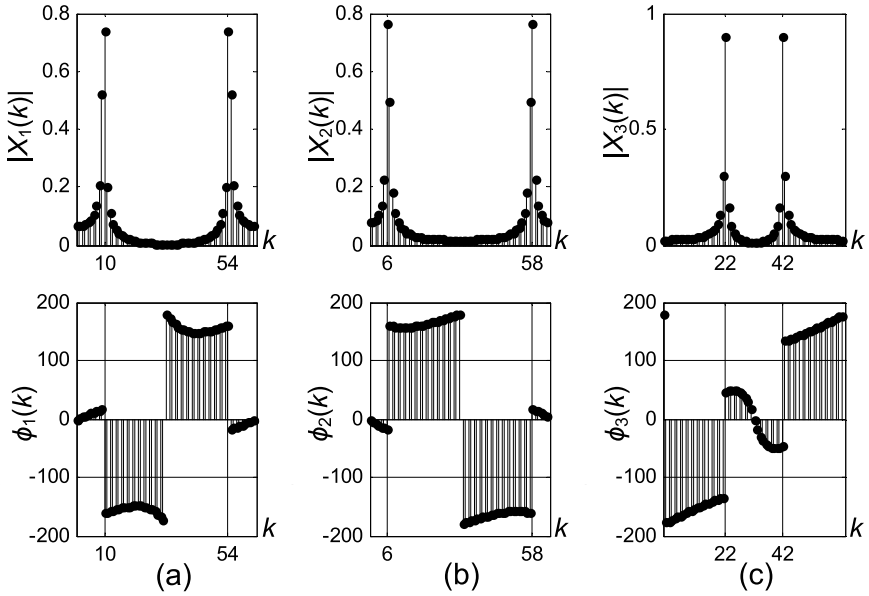

FIGURE 3. Magnitude and phase spectra plot. (a) Channel 1 (with the sampling rate f_{s1}). (b) Channel 2 (with the sampling rate f_{s2}). (c) Channel 3 (with the sampling rate f_{s3}).

TABLE 1. Observed peak phases and corrected peak phases of two side spectra.

Channel	$i=1$		$i=2$		$i=3$	
Peak index	$k_{i,L}$	$k_{i,R}$	$k_{i,L}$	$k_{i,R}$	$k_{i,L}$	$k_{i,R}$
	10	54	6	58	22	42
Observed $\phi_{i,k}$	$-161.30°$	$161.30°$	$-17.27°$	$17.27°$	$47.08°$	$-47.08°$
$\hat{\delta}_i$	-0.4010		0.4021		-0.2400	
Corrected $\hat{\varphi}_{i,k}$	$-90.25°$	$90.25°$	$-88.52°$	$88.52°$	$89.60°$	$-89.60°$
Recognized $\hat{k}_i$	54		58		22	
$\hat{r}_i$	108.8020		172.7936		108.8002	
$\hat{f}_0$	748.7986Hz					

Maroosi-Bizaki estimator in [4]. The distinctions between this estimator and our proposed estimator are as the follows.

1) The Maroosi-Bizaki estimator can directly recover the frequency using multiple undersampled sequences without any extra hardware circuit, while our proposed estimator needs a simple circuit to detect the zero crossing point of the input analog signal. Hence, the proposed scheme obviously depends on the detection accuracy of the crossing point "O".

2) As [4] pointed out, compared to the determination case of complex exponential waveforms, the Maroosi-Bizaki estimator is at the cost of lowering the upper bound for unambiguous frequency detection. In contrast, by means of zero-crossing detection and remainder sifting, our proposed estimator actually transforms the frequency determination for a real-valued sinusoidal signal into that for a complex exponential signal. Hence, our estimator shares the same upper bound of frequency recovery (calculated by (9), i.e., the least common multiple of all moduli) with the estimators in [11] and [19]. Specifically, for the 3 undersampling rates $f_{s1} = 128$Hz, $f_{s2} = 192$Hz, $f_{s3} = 320$Hz in *Example 1*, one can calculate the upper bounds of frequency recovery for the Maroosi-Bizaki estimator (see [4]) and the proposed estimator as 352Hz, 1920Hz, respectively. As a result, the frequency $f_0 = 748.8$Hz cannot be recovered by the Maroosi-Bizaki estimator since it exceeds the upper bound 352Hz.

3) The complexity of the proposed estimator is lower than the Maroosi-Bizaki estimator and the estimator in [6], since the former can acquire a closed-form solution following the aforementioned procedure, in which no searching operations are involved. In contrast, the estimators proposed in [4]–[6] cannot work in a closed-form way and their solutions are acquired through searching out the optimal case among quantities of remainder combinations.

IV. NUMERICAL RESULTS

This section aims to investigate the root-mean-square error (RMSE) of the proposed frequency estimator under different SNR (signal-to-noise ratio) levels, and compare it with the Maroosi-Bizaki estimator.

Example 2: In this example, the comparison between our proposed estimator and the Maroosi-Bizaki estimator is presented. Consider a real-valued analog signal

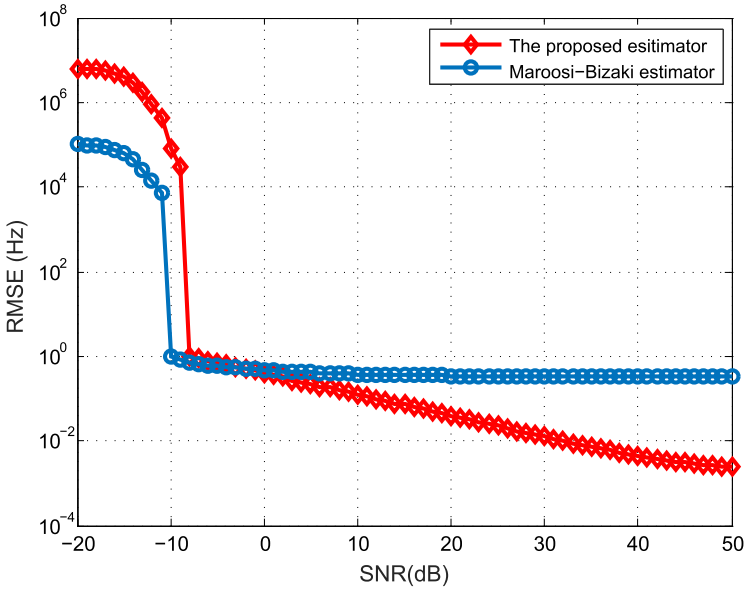

FIGURE 4. RMSE curves of the proposed estimator and the Maroosi-Bizaki estimator.

$x(t) = \cos(2\pi f_0 t + \pi/2)$, $f_0 = 193000$Hz. Specify the DFT size $N = 800$. Moreover, these two estimators share $L = 3$ common undersampling rates as $f_{s1} = 18400$Hz, $f_{s2} = 19200$Hz, $f_{s3} = 20000$Hz. Hence, our proposed estimator's co-prime integer set $\{\Gamma_1, \Gamma_2, \Gamma_3\} = \{23, 24, 25\}$ (since $\Gamma_i = f_{si}/N, i = 1, \cdots, L$).

In terms of (9), the upper bound of frequency recovery equals $N\Gamma_1\Gamma_2\Gamma_3 = 11040000$Hz, whereas the upper bounds of the Maroosi-Bizaki estimator (calculated by (3) in [4]) and the three-channel estimator (calculated by $\Gamma_1\Gamma_2\Gamma_3$, as [6] proved) are 230800Hz and 13800Hz, respectively. Thus, the original signal's frequency $f_0 = 193000$Hz can be retrieved by both the proposed estimator and Maroosi-Bizaki estimator. However, it cannot be recovered by the three-channel estimator in [6], since f_0 exceeds its upper bound 13800Hz and this estimator is on basis of the complex-valued model rather than the real-valued model.

To compare these two estimators' noise robustness and accuracy, a SNR range varying from −20dB to 50dB was taken into account. In each SNR case, 1000 Monte Carlo trials were conducted. Fig. 4 illustrates their RMSE curves.

From Fig. 4, the following 2 conclusions can be drawn:

1) In the low SNR region, the Maroosi-Bizaki estimator outperforms our proposed estimator in the noise robustness, since their anti-noise SNR thresholds are −10dB, −8dB, respectively. This is because, for our estimator, the zero-crossing moment detected by the triggering circuit tends to be sensitive to heavy noise, which does not exist in the Maroosi-Bizaki estimator.

2) In the high SNR region, the RMSEs of Maroosi-Bizaki estimator are slightly greater than our proposed estimator, demonstrating that the adoption of CRT and spectrum correction tends to yield a high recovery accuracy.

Example 3: This example aims to investigate our proposed estimator's accuracy when f_0 is greater than the upper bound of Maroosi-Bizaki estimator. Consider a real-valued analog signal $x(t) = 2\cos(2\pi f_0 t + \pi/2), f_0 = 5990.4$ Hz. Specify the DFT size $N = 512$, the co-prime integer set $\{\Gamma_1, \Gamma_2, \Gamma_3\} = \{2, 3, 5\}$ and thus the sampling rates of the $L = 3$ ADCs are $f_{s1} = 1024$Hz, $f_{s2} = 1536$Hz, $f_{s3} = 2560$Hz (since $N = \gcd\{f_{s1}, \cdots, f_{sL}\} = 512$). Clearly, the original frequency $f_0 = 5990.4$ Hz exceeds the upper bound of both the Maroosi-Bizaki estimator (i.e., 2816Hz calculated by (3) in [4]) and the upper bound of the three-channel estimator in [6] (i.e., $\Gamma_1\Gamma_2\Gamma_3 = 30$Hz).

Note that, since the estimators addressed in [7], [11], [12], and [3], [18], [19] can only deal with complex-valued signals, it is impossible to compare them with the proposed estimator in this case of real-valued signals.

To investigate the proposed estimator's robustness to noises, a SNR range varying from −15dB to 20dB was taken into account. In each SNR case, 1000 Monte Carlo trials were conducted. The RMSE curve is illustrated in Fig. 5.

From Fig. 5, we can draw that the proposed estimator also possesses high accuracy. Specifically, in any SNR region above the threshold, the RMSE is less than 0.1Hz, i.e., the relative error is smaller than 0.002% since the true frequency is 5990.4Hz.

The high accuracy lies in 3 reasons: Firstly, the proposed remainder sifting approach makes the CRT-based estimator feasible to deal with real-valued signals; Secondly, as [16] and [19] pointed out, the closed-form CRT itself does not generate additional reconstruction error; Lastly, the Candan spectrum corrector can provide a high-accuracy estimate of the frequency offset.

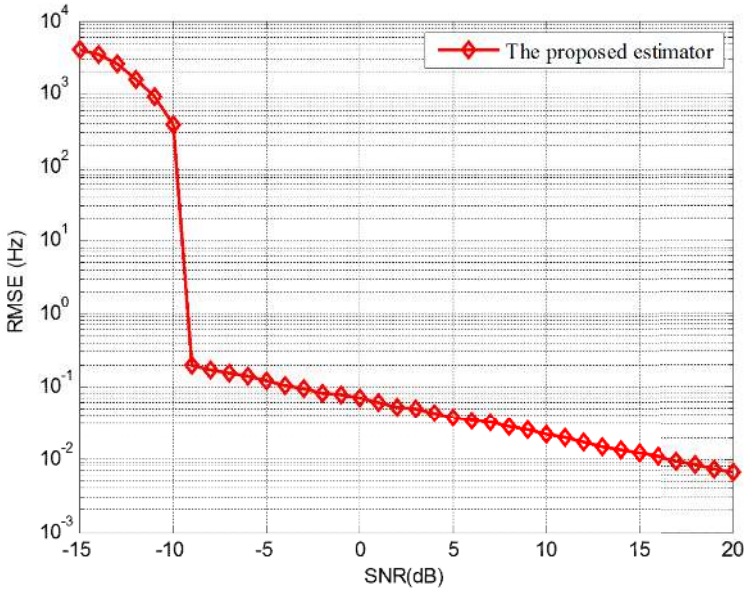

FIGURE 5. RMSE curve of the proposed estimator (Candan corrector is incorporated).

In addition, the evaluation of an estimator's accuracy is based on the comparison between the estimation error variance with the Cramer-Rao lower bound (CRB). As far as the frequency estimation is concerned, D.C.Rife provided a well-known CRB analytic expression in [23], which only applies for the single-path Nyquist sampling case. As to the CRB for the undersampling case across multiple channels, many researchers recently put forward different opinions (see [24]–[27]). However, up to now, they have not come to a unified conclusion. As a result, the deduction of an analytic CRB expression for multiple-channel undersampling case is still an open topic.

V. CONCLUSIONS

This paper proposed a novel frequency estimator for undersampled real-valued sinusoidal waveforms, which widens the application range of the existing CRT-based frequency estimators. Due to the incorporation of Closed-form CRT, spectrum correction and crossing point circuit triggering, our proposed estimator concurrently possesses the merits of large frequency recovery range, low computational complexity, and high accuracy. Therefore, The proposed estimator is hopeful to be applied to those fields involving the frequency estimation of undersampled waveforms such as mobile communication, spectrum sensing in cognitive radio etc.

The future work focuses on two aspects: 1) Make endeavor to deal with a real-valued undersampled waveform containing multiple components [28]–[30], which requires more creative work on remainder sifting, remainder paring, remainder classification etc. 2) Efforts should also be made to improve the accuracy at the low SNR region, which seems to a bit inferior to the Maroosi-Bizaki estimator.

REFERENCES

[1] B. Friedlander and B. Porat, "VSAR: A high resolution radar system for ocean imaging," *IEEE Trans. Aerosp. Electron. Syst.*, vol. 34, no. 3, pp. 755–776, Jul. 1998.

[2] Y. Zhang, M. Amin, and F. Ahmad, "Time-frequency analysis for the localization of multiple moving targets using dual-frequency radars," *IEEE Signal Process. Lett.*, vol. 15, pp. 777–780, Nov. 2008.

[3] X. Li and X.-G. Xia, "A fast robust Chinese remainder theorem based phase unwrapping algorithm," *IEEE Signal Process. Lett.*, vol. 15, pp. 665–668, Nov. 2008.

[4] A. Maroosi and H. K. Bizaki, "Digital frequency determination of real waveforms based on multiple sensors with low sampling rates," *IEEE Sensors J.*, vol. 12, no. 5, pp. 1483–1495, May 2012.

[5] A. Maroosi and H. K. Bizaki, "Multiple frequencies determination of sinusoidal real waveform by multiple sensors with low sampling rate," *IEEE Sensors J.*, vol. 17, no. 24, pp. 8404–8411, Dec. 2017.

[6] H. Shan, H. Zhang, S. Hong, Y. Lei, and L. Chen, "Frequency estimation of multiple sinusoids with three sub-Nyquist channels," *Signal Process.*, vol. 139, pp. 96–101, Oct. 2017.

[7] X.-G. Xia, "On estimation of multiple frequencies in undersampled complex valued waveforms," *IEEE Trans. Signal Process.*, vol. 47, no. 12, pp. 3417–3419, Dec. 1999.

[8] P. P. Vaidyanathan and P. Pal, "Sparse sensing with co-prime samplers and arrays," *IEEE Trans. Signal Process.*, vol. 59, no. 2, pp. 573–586, Feb. 2011.

[9] P. P. Vaidyanathan, "Analog filter banks for sampling: Discretization, polyphase form, and role in compressive sensing," in *Proc. IEEE Digit. Signal Process. Signal Educ. Meeting (DSP/SPE)*, Aug. 2013, pp. 24–29.

[10] X. Huang, Z. Yan, S. Jing, H. Fang, and L. Xiao, "Co-prime sensing-based frequency estimation using reduced single-tone snapshots," *Circuits, Syst., Signal Process.*, vol. 35, no. 9, pp. 3355–3366, 2016.

[11] X. Li, H. Liang, and X.-G. Xia, "A robust Chinese remainder theorem with its applications in frequency estimation from undersampled waveforms," *IEEE Trans. Signal Process.*, vol. 57, no. 11, pp. 4314–4322, Nov. 2009.

[12] G. Li, J. Xu, Y. N. Peng, and X. G. Xia, "An efficient implementation of a robust phase-unwrapping algorithm," *IEEE Signal Process. Lett.*, vol. 14, no. 6, pp. 393–396, Jun. 2007.

[13] L. Xiao, X.-G. Xia, and H. Huo, "Towards robustness in residue number systems," *IEEE Trans. Signal Process.*, vol. 65, no. 6, pp. 1497–1510, Mar. 2017.

[14] L. Xiao and X.-G. Xia, "A new robust Chinese remainder theorem with improved performance in frequency estimation from undersampled waveforms," *Signal Process.*, vol. 117, pp. 242–246, Dec. 2015.

[15] L. Xiao, X.-G. Xia, and W. Wang, "Multi-stage robust Chinese remainder theorem," *IEEE Trans. Signal Process.*, vol. 62, no. 18, pp. 4772–4785, Sep. 2014.
[16] W. Wang, X. Li, W. Wang, and X.-G. Xia, "Maximum likelihood estimation based robust chinese remainder theorem for real numbers and its fast algorithm," *IEEE Trans. Signal Process.*, vol. 63, no. 13, pp. 3317–3331, Jul. 2015.
[17] L. Xiao and X.-G. Xia, "Frequency determination from truly sub-Nyquist samplers based on robust Chinese remainder theorem," *Signal Process.*, vol. 150, pp. 248–258, Sep. 2018.
[18] X.-G. Xia and G. Wang, "Phase unwrapping and a robust Chinese remainder theorem," *IEEE Signal Process. Lett.*, vol. 14, no. 4, pp. 247–250, Apr. 2007.
[19] W. Wang and X.-G. Xia, "A closed-form robust Chinese remainder theorem and its performance analysis," *IEEE Trans. Signal Process.*, vol. 58, no. 11, pp. 5655–5666, Nov. 2010.
[20] B. G. Quinn, "Estimating frequency by interpolation using Fourier coefficients," *IEEE Trans. Signal Process.*, vol. 42, no. 5, pp. 1264–1268, May 1994.
[21] C. Candan, "Analysis and further improvement of fine resolution frequency estimation method from three DFT samples," *IEEE Signal Process. Lett.*, vol. 20, no. 9, pp. 913–916, Sep. 2013.
[22] X. Huang and X. G. Xia, "A fine resolution frequency estimator based on double sub-segment phase difference," *IEEE Signal Process. Lett.*, vol. 22, no. 8, pp. 1055–1059, Aug. 2015.
[23] D. C. Rife and R. R. Boorstyn, "Single tone parameter estimation from discrete-time observations," *IEEE Trans. Inf. Theory*, vol. IT-20, no. 5, pp. 591–598, Sep. 1974.
[24] A. Koochakzadeh and P. Pal, "Cramér–Rao bounds for underdetermined source localization," *IEEE Signal Process. Lett.*, vol. 23, no. 7, pp. 919–923, Jul. 2016.
[25] C.-L. Liu and P. P. Vaidyanathan, "Cramé–Rao bounds for coprime and other sparse arrays, which find more sources than sensors," *Digit. Signal Process.*, vol. 61, pp. 43–61, Feb. 2017.
[26] S. Qin, Y. D. Zhang, M. G. Amin, and A. M. Zoubir, "Generalized coprime sampling of toeplitz matrices for spectrum estimation," *IEEE Trans. Signal Process.*, vol. 65, no. 1, pp. 81–94, Jan. 2017.
[27] M. Wang and A. Nehorai, "Coarrays, MUSIC, and the Cramér–Rao bound," *IEEE Trans. Signal Process.*, vol. 65, no. 4, pp. 933–946, Feb. 2017.
[28] J. Lerga, V. Sucic, and B. Boashash, "Multicomponent noisy signal adaptive instantaneous frequency estimation using components time support information," *IET Signal Process.*, vol. 8, no. 3, pp. 277–284, May 2014.
[29] J. Lerga, V. Sucic, and B. Boashash, "An improved method for nonstationary signals components extraction based on the ICI rule," in *Proc. Int. Workshop Syst., Signal Process. Appl.*, May 2011, pp. 307–310.
[30] J. Lerga and V. Sucic, "An instantaneous frequency estimation method based on the improved sliding pair-wise ICI rule," in *Proc. Int. Conf. Sci. Signal Process. Appl.*, May 2010, pp. 161–164.

XIANGDONG HUANG was born in 1979. He received the M.S. and Ph.D. degrees from Tianjin University, Tianjin, China, in 2004 and 2007, respectively, where he is currently an Associate Professor with the School of Electrical and Information Engineering. In 2009, he was with The University of Hong Kong, as a Visiting Scholar. In 2011, he was with the University of Macau, as a Research Assistant. In 2013, he was with the University of Delaware, as a Visiting Scholar. His research interests include filter design and spectral analysis.

HUIJIE WANG was born in 1994. He received the bachelor's degree from Tianjin University, Tianjin, China, in 2017, where he is currently pursuing the M.S. degree with the School of Electrical and Information Engineering. His research interests include the algorithm in 5G and spectrum correction.

HAOHUA QIN was born in 1979. He received the M.S. degree from Tianjin Polytechnic University, in 2004. He is currently an Associate Professor with the College of Automation and Electronic Engineering, Qingdao University of Science and Technology, Qindao, China. His research interests include embedded system design and machine vision.

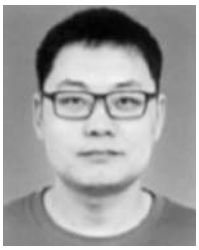

WEIZHI NIE received the B.S. and M.S. degrees in electronic engineering from Tianjin University, China, where he is currently pursuing the Ph.D. degree. His research interests include multiple object tracking, computer vision, and location-based social networks.